Bone 124 (2019) 148–157

Contents lists available at ScienceDirect

Bone

journal homepage: www.elsevier.com/locate/bone

Full Length Article

Abaloparatide improves cortical geometry and trabecular microarchitecture and increases vertebral and femoral neck strength in a rat model of male osteoporosis☆

Tatiana Besschetnova[a], Daniel J. Brooks[b], Dorothy Hu[c], Kenichi Nagano[c], Jordan Nustad[b], Michael Ominsky[a], Bruce Mitlak[a], Gary Hattersley[a], Mary L. Bouxsein[b,d], Roland Baron[c,e], Beate Lanske[a,*]

[a] Radius Health, Waltham, MA, USA
[b] Center for Advanced Orthopaedic Studies, Beth Israel Deaconess Medical Center, Boston, MA, USA
[c] Division of Bone and Mineral Research, Dept of Oral Medicine, Infection and Immunity, Harvard School of Dental Medicine, Boston, MA, USA
[d] Department of Orthopaedic Surgery, Harvard Medical School, Boston, MA, USA
[e] Harvard Medical School and Endocrine Unit, Massachusetts General Hospital, Boston, MA, USA

ARTICLE INFO

Keywords:
Hypogonadism
Anabolic
Bone formation
PTH receptor agonist
Androgen deficiency
Bone strength

ABSTRACT

Androgen deficiency is a leading cause of male osteoporosis, with bone loss driven by an inadequate level of bone formation relative to the extent of bone resorption. Abaloparatide, an osteoanabolic PTH receptor agonist used to treat women with postmenopausal osteoporosis at high risk for fracture, increases bone formation and bone strength in estrogen-deficient animals without increasing bone resorption. This study examined the effects of abaloparatide on bone formation, bone mass, and bone strength in androgen-deficient orchiectomized (ORX) rats, a male osteoporosis model. Four-month-old Sprague-Dawley rats underwent ORX or sham surgery. Eight weeks later, sham-operated rats received vehicle (saline; $n = 10$) while ORX rats (n = 10/group) received vehicle (Veh) or abaloparatide at 5 or 25 μg/kg (ABL5 or ABL25) by daily s.c. injection for 8 weeks, followed by sacrifice. Dynamic bone histomorphometry indicated that the tibial diaphysis of one or both abaloparatide groups had higher periosteal mineralizing surface, intracortical bone formation rate (BFR), endocortical BFR, and cortical thickness vs Veh controls. Vertebral trabecular BFR was also higher in both abaloparatide groups vs Veh, and the ABL25 group had higher trabecular osteoblast surface without increased osteoclast surface. By micro-CT, the vertebra and distal femur of both abaloparatide-groups had improved trabecular bone volume and micro-architecture, and the femur diaphysis of the ABL25 group had greater cortical thickness with no increase in porosity vs Veh. Biomechanical testing indicated that both abaloparatide-groups had stronger vertebrae and femoral necks vs Veh controls. These findings provide preclinical support for evaluating abaloparatide as an investigational treatment for male osteoporosis.

1. Introduction

Abaloparatide is a novel and selective parathyroid hormone receptor (PTHR) agonist [1,2] that reduces the risk of osteoporotic fractures in postmenopausal women by increasing bone formation and bone mineral density (BMD) [3,4]. Rodent and non-human primate models of postmenopausal osteoporosis show that abaloparatide increases BMD by stimulating bone formation on endocortical, periosteal, and trabecular bone surfaces without increasing bone resorption [5–7]. These cellular responses to abaloparatide, and the attendant improvements in bone mass, bone volume, trabecular microarchitecture, and cortical geometry, are associated with increased strength of the vertebrae [5,6], femoral diaphysis [6], and femoral neck [6] of estrogen-deficient ovariectomized (OVX) animals.

Male forms of osteoporosis bear many of the hallmarks of postmenopausal osteoporosis, along with some distinctions. One distinction is that men tend to develop higher fragility fracture risk around ten years later than women due to mens' higher average peak bone mass

☆ Some of these data were presented in abstract form at the annual meeting of the American Society for Bone and Mineral Research, Montreal, Canada, Sept. 28–Oct. 1, 2018.

* Corresponding author at: Radius Health Inc., 950 Winter Street, Waltham, MA 02451, USA.
E-mail address: blanske@radiuspharm.com (B. Lanske).

https://doi.org/10.1016/j.bone.2019.04.025
Received 23 December 2018; Received in revised form 26 April 2019; Accepted 29 April 2019
Available online 30 April 2019

[8]. However, life expectancy is increasing more for men than for women, leading more men to reach advanced ages that are associated with exponentially higher fracture risk [9,10]. Bone loss in older men may be related in part to low estradiol levels, driven by reduced levels of the androgen testosterone, an estradiol precursor [11]. Testosterone levels abruptly decline in men undergoing surgical (orchiectomy, ORX) or medical androgen deprivation therapy for prostate cancer [12], often leading to rapid bone loss and increased fracture risk [13]. Testosterone levels also tend to gradually decline with age in older men [14], often due to co-morbid conditions [15], and these forms of hypogonadism represent a significant cause of secondary male osteoporosis [16]. Some evidence suggests that average serum testosterone levels in American men have been in decline over the past few decades at a population level [17], independent of aging, which may further increase the population of older men at risk of bone loss and fragility fractures. Androgen deficiency is associated with a higher risk for falls, which may further increase fracture risk beyond the adverse effects of androgen deficiency on bone mass and strength [18]. Around 40% of all fragility fractures occur in men [19], and mortality after fragility fractures in general [20] and hip fractures in particular [21] is higher for men than for women, yet < 10% of men with new fragility fractures are prescribed an osteoporosis medication [22].

At a cellular level, male osteoporosis often arises from increased bone resorption and bone formation that is either suppressed or insufficiently increased to counter higher bone resorption [11,18]. Antiresorptive therapies including bisphosphonates and denosumab increase bone mass and strength but do not reverse deficits in bone formation that may occur in men with osteoporosis, limiting their potential to reverse degraded bone microarchitecture and geometry. The PTHR agonist teriparatide increases lumbar spine and femoral neck BMD in men with osteoporosis by increasing bone formation, but teriparatide also increases bone resorption, which may limit its bone-building potential at certain sites, including the hip [23]. There remains an unmet need among men with osteoporosis for therapeutic options that can stimulate bone formation with minimal stimulation of bone resorption, a pharmacodynamic profile that abaloparatide exhibits in estrogen-deficient states [3,5,7]. Recent cell culture studies suggest that abaloparatide may cause smaller or more transient increases in the pro-resorptive cytokine receptor activator of nuclear factor kappa-B ligand (RANKL) compared with the effects of teriparatide [24,25]. Those findings may be noteworthy because RANKL levels are elevated in the blood and bone marrow of ORX rats, and increased RANKL has been implicated as a cause of ORX-induced bone loss [26,27].

A recent study in osteopenic ORX rats showed that abaloparatide improved trabecular BMD by stimulating bone formation without increasing bone resorption [28]. The current report extends that study's findings by describing the effects of abaloparatide on cortical bone histomorphometry endpoints, micro-computed tomography (micro-CT) parameters of cortical and trabecular bone, and biomechanical properties of the femoral neck, femoral diaphysis, and lumbar vertebrae in ORX rats.

2. Materials and methods

2.1. Animals and study design

All animal procedures and activities were approved by Charles River Montreal's Institutional Animal Care and Use Committee and were performed in an AAALAC-accredited vivarium at Charles River Laboratories, Montreal, Quebec, Canada. Animal care and study design features of the experiment were described previously [28]. Briefly, 30 male Sprague-Dawley rats underwent ORX surgery at 4 months of age and 10 similar rats underwent a sham surgical procedure, followed by an 8-week recovery period to allow bone depletion in the ORX animals. The ORX animals were then allocated to 3 groups of 10 animals balanced for body weight and lumbar spine areal bone mineral density (aBMD) by dual X-ray absorptiometry (DXA). The ORX groups then received daily s.c. injections of vehicle (0.9% sodium chloride; Veh) or abaloparatide (Radius Health) at 5 μg/kg/d (ABL5) or 25 μg/kg/d (ABL25) for 8 weeks. The sham control rats received daily s.c. vehicle injections. All rats received a single s.c. injection of alizarin complexone (25 mg/kg; A3882, Sigma) one week prior to the start of dosing and s.c. injections of calcein green (8 mg/kg; C0875, Sigma) on the 10th and 3rd day prior to sacrifice. Food consumption and body weights were monitored regularly throughout the study. Rats were sacrificed by exsanguination from the abdominal aorta after isoflurane anesthesia.

2.2. Bone histomorphometry

The right tibia and the 3rd lumbar vertebra (L3) from 8 randomly-selected animals per group were fixed in 10% neutral buffered formalin for 3 days and transferred to 70% ethanol for storage. A handsaw (Dremel 426 Cut-off wheel) was used to bisect the tibial diaphysis at the mid-point between the proximal and distal tibiofibular junctions. The proximal and distal portion of the tibia and L3 were then dehydrated with graded ethanol, cleared with xylene, and embedded undecalcified in methylmethacrylate. Consecutive sagittal sections of the proximal portion of the tibia, transverse sections of the diaphyseal region of the distal portion of the tibia, and frontal sections through the middle of the of L3 vertebral body were cut at 5-μm thickness with an RM2255 microtome (Leica, Germany). Sections were stained with von Kossa to reveal mineralized bone matrix, or with toluidine blue (pH 3.7) for osteoid and cellular parameters.

The tibial diaphysis cortical bone histomorphometric dynamic parameters were analyzed under 100× magnification in a region of up to 21.06 mm^2, and at 20× magnification for structural data analyzed in a 4.5 mm by 6.5 mm region. The vertebral sections were analyzed under 200× magnification within a 1.95 mm by 2.25 mm region of cancellous bone at a fixed distance (500 μm) from the growth plates that avoided primary spongiosa.

Structural parameters for the proximal tibial included bone volume per tissue (i.e. bone plus marrow) volume (BV/TV), trabecular thickness (Tb.Th), trabecular number (Tb.N), and trabecular separation (Tb.Sp). Structural parameters for the tibial diaphysis included total area (T.Ar), cortical bone area (Ct. Ar), cortical marrow area (Ma.Ar), cortical BV/TV (Ct.BV/TV), cortical thickness (Ct.Th), cortical porosity (Ct.Po), and endocortical perimeter (Ec.Pm). Periosteal perimeter (Ps.Pm) was determined from a single toluidine blue section, whereas all other cortical and trabecular structural parameters were determined from two serial sections, one von Kossa-stained and one Toluidine blue-stained, the results of which were averaged. Pores were included in cortical porosity measurements if they had a minimal diameter of 70 ± 20 μm and were not contiguous with marrow space in the sectioning plane. Cellular parameters evaluated in vertebral trabecular bone included osteoblast surface per bone surface (Ob.S/BS), osteoblast number per bone perimeter (N.Ob/B.Pm), osteoclast surface per bone surface (Oc.S./BS), osteoclast number per bone perimeter (N.Oc/B.Pm), osteoid surface per bone surface (OS/BS), and osteoid thickness (O.Th). Additional tibial and vertebral sections were mounted unstained for assessments of fluorescence-based dynamic parameters, including mineral apposition rate (MAR), mineralizing surface (MS/BS), bone formation rate per bone surface (BFR/BS), BFR per volume (BFR/BV), and tibial intracortical BFR. Intracortical BFR was assessed within intracortical pores of at least 70 ± 20 μm in diameter that were not contiguous with marrow space within the plane of sectioning. Sections were analyzed with a Nikon E800 microscope equipped with an Olympus DP71 digital camera that captured images via Olympus CellSens software. Data were obtained using OsteoMeasure software (Osteometrics Inc., Decatur, GA, USA) and standardized bone histomorphometry analyses and nomenclature [29].

2.3. Micro-computed tomography

The whole right femur and L4 vertebra were collected at necropsy and scanned with a high-resolution desktop micro-CT imaging system (μCT40, Scanco Medical AG, Bruttisellen, Switzerland). Scans were acquired using a 15 μm isotropic voxel size, with 70 kVp peak X-ray tube potential, 114 mA·s tube current, and 300 ms integration time, and subjected to Gaussian filtration and segmentation. Image acquisition and analysis protocols adhered to published guidelines for the assessment of rodent bones by micro-CT [30].

Cortical bone was analyzed in 75 transverse micro-CT slices comprising a region of interest (ROI) of 1.125 mm in length at the femoral mid-diaphysis, with the ROI comprising all tissue within the outermost edge of the cortex. Images were subjected to Gaussian filtration and were segmented using a fixed threshold of 700 mg hydroxyapatite/cm^3. The following variables were computed: total area (cross-sectional bone area, including marrow; Tt.Ar), cortical bone area (B.Ar), marrow area (Ma.Ar), cortical bone area per total area (B.Ar/Tt.Ar), cortical tissue mineral density (Ct.TMD), cortical thickness (Ct.Th), cortical porosity (Ct.Po), and polar moment of inertia (pMOI). Total femur length was also determined from the micro-CT scans.

Trabecular bone was analyzed in the distal femur and L4 vertebral body. L4 trabecular bone was analyzed within an ROI that extended from 150 μm inferior the cranial endplate to 150 μm superior to the caudal end-plate. The contours of this auto-contoured boundary were manually corrected where it did not run parallel to the endocortical surface or otherwise touched the cortex or areas of the growth plates. Whole cross-sections of the distal L4 vertebral body (cortex and trabecular bone) were also analyzed for total bone area (Tt.B.Ar) total bone area per total area (Tt.B.Ar/Tt.Ar), and total volumetric BMD (Tt.vBMD). For the distal femur, transverse micro-CT slices were evaluated in an ROI beginning 600 μm proximal to the most proximal aspect of the distal growth plate and extending proximally 3 mm (200 slices). Trabecular regions were identified by semi-manually contouring the trabecular bone within the ROI with the assistance of an auto-thresholding software algorithm. Images were thresholded using an adaptive-iterative algorithm, with the average thresholds of the ABL25 group (550 mg hydroxyapatite/cm^3 and 500 mg hydroxyapatite/cm^3 for the femur and L4, respectively) used to segment bone from soft tissue in all groups. Trabecular parameters included trabecular BV/TV (Tb.BV/TV), trabecular vBMD (Tb.vBMD), trabecular thickness (Tb.Th), trabecular number (Tb.N), trabecular separation (Tb.Sp), connectivity density (Conn.D), and structure model index (SMI).

2.4. Bone biomechanics

Whole femur three-point bending tests, femoral neck shear tests, and vertebral body compression tests were conducted using a servo-hydraulic material testing machine (Model 8511, Instron, Norwood, MA). The three-point bending tests were performed with the anterior surface of the femur resting on the bottom supports (span length = 20 mm) and the central load point moving at a rate of 3 mm/min until the bone fractured, with force and displacement data collected at 100 Hz. Ultimate load, stiffness, and work to fracture were determined from the force-displacement curves using MATLAB (Version R2017a), with work to fracture comprising the area under the curve as determined by the Riemann Sum method. Estimated femoral diaphyseal material properties were calculated based on force-displacement data and micro-CT-derived mid-shaft geometry: Apparent ultimate stress was a function of $(P * L * c) / 4I$, where P is peak load (N), L is span length between lower supports (mm), c = radius (mm), and I is moment of inertia (mm^4); apparent elastic modulus was a function of $(m * L^3) / 48I$, where m is the secant slope of the linear region of the load-deformation curve; apparent toughness was a function of $(0.75Wb^2)/LI$, where W is work to fracture (mJ).

Following the bending test, the proximal end of the femur was prepared for femoral neck shear testing by potting the diaphyseal end in polymethyl methacrylate. The potted sample was clamped in a three-point lathe chuck at the base of the testing machine and an axial load was applied to the top of the femoral head at a rate of 6 mm/min until failure. Stiffness, ultimate force, and work to fracture were determined from the load-displacement curves.

For vertebral compression tests, the end-plates and posterior and transverse elements of the L4 vertebral body were removed using a low-speed diamond saw (Isomet 1000, Buehler, Lake Bluff, IL), thereby creating samples with a uniform 5 mm height and planoparallel ends. Samples were then loaded in compression between flat platens at a rate of 1 mm/min. Force and displacement data were used to determine stiffness, ultimate force, and work to ultimate load of each sample.

2.5. Statistics

Histomorphometry, micro-CT, and bone biomechanics data were analyzed by one-way ANOVA. If the ANOVA test was significant, Tukey's post-test was applied to compare all groups against each other. These analyses, as well as linear regression analyses, were performed using Prism GraphPad V8. For all statistical tests, a P value < 0.05 was used to indicate significant differences.

3. Results

3.1. General health

All animals survived in good health until scheduled necropsy, at which time the effectiveness of ORX surgery was confirmed by the lack of epididymis and testes. An androgen deprivation effect of ORX was supported by a 10.4% deficit in body weight gain in the ORX groups vs Sham controls at the end of the 8-week bone depletion period (data not shown). Treatments were well-tolerated, and abaloparatide had no effect on food consumption or body weight gain (data not shown; Radius Health data on file).

3.2. Bone histomorphometry

Histomorphometry of the tibial diaphysis indicated ORX-related deficits in cortical bone mass, with significantly lower T.Ar, Ps.Pm, and Ct.Ar in the Veh group vs Sham controls (Table 1 and Fig. 1). Ma.Ar was significantly lower in the Veh group vs Sham controls (Fig. 1). Abaloparatide had positive effects on several parameters of cortical bone structure, with significantly greater Ct.Ar, Ct.BV/TV, and Ct.Th in one or both abaloparatide groups compared with Veh controls (Fig. 1). Abaloparatide had no notable effects on Ps.Pm (Table 1). The ABL25 group had significantly greater endocortical MAR and BFR/BS vs both Veh and Sham controls (Fig. 1F and I). The abaloparatide-related increase in endocortical MAR is evident by the greater distance between the alizarin red and calcein green labels shown in Fig. 2D vs Fig. 2A and B. Endocortical BFR/BV was similar in the abaloparatide and Veh groups (Fig. 1H). Periosteal MS/BS, periosteal BFR/BV, and periosteal BFR/BS were all significantly lower in the Veh group vs Sham controls, and the ABL25 group showed significantly greater periosteal MS/BS compared with Veh (Table 1). The ABL25 group also had significantly greater intracortical BFR vs all other groups (Table 1). Cortical porosity (Ct.Po) was statistically similar in all four groups (Table 1).

Trabecular bone histomorphometry for the L3 vertebral body showed that the Veh group had significantly higher osteoid surface per bone surface (OS/BS) (Table 1) compared with Sham controls, whereas other indices of L3 trabecular bone formation and bone structure were not significantly affected by ORX. Both abaloparatide groups had significantly greater Tb.BV/TV, Tb.Th, and trabecular number (Tb.N) compared with Veh controls, and Tb.Sp was significantly lower in both abaloparatide groups vs Veh (Fig. 3A–D). These structural differences are evident in von Kossa-stained photomicrographs shown in Fig. 2F–H.

Table 1
Bone histomorphometry data for tibial diaphysis cortical bone and L3 trabecular bone (see Figs. 1 and 3 for additional endpoints). Data represent means ± SEM, $N = 8$/group.

	Sham	Veh	ABL5	ABL25
Tibial diaphysis cortical bone				
Total area (T.Ar, mm^2)	11.00 ± 0.41	8.61 ± 0.34^	9.22 ± 0.38^	9.12 ± 0.32^
Periosteal perimeter (Ps.Pm, mm)	14.14 ± 0.18	12.80 ± 0.25^	13.29 ± 0.28	13.57 ± 0.35
Periosteal MAR (μm/d)	1.27 ± 0.15	0.80 ± 0.10	0.92 ± 0.09	1.09 ± 0.19
Periosteal MS/BS (%)	46.56 ± 5.05	26.9 ± 3.98^	31.88 ± 3.14	43.15 ± 3.67*
Periosteal BFR/BS ($\mu m^3/\mu m^2$/d)	0.60 ± 0.11	0.23 ± 0.05^	0.30 ± 0.05	0.46 ± 0.09
Periosteal BFR/BV (%/year)	0.126 ± 0.021	0.052 ± 0.012^	0.062 ± 0.010	0.093 ± 0.018
Intracortical BFR/BV (%/year)	2.12 ± 0.35	2.07 ± 0.62	1.79 ± 0.29	4.66 ± 0.76*^+
Cortical porosity (Ct.Po, %)	0.226 ± 0.066	0.204 ± 0.092	0.137 ± 0.024	0.267 ± 0.055
L3 vertebral body trabecular bone				
Osteoblast surface per bone surface (Ob.S/BS, %)	2.33 ± 0.76	5.16 ± 0.57	5.69 ± 0.74^	9.47 ± 1.16*^+
Osteoid surface per bone surface (OS/BS, %)	0.79 ± 0.38	3.05 ± 0.46^	1.78 ± 0.38	2.71 ± 0.73
Osteoid Thickness (O.Th, μm)	2.69 ± 0.61	3.19 ± 0.09	3.38 ± 0.25	3.42 ± 0.18
Osteoclast surface per bone surface (Oc.S/BS, %)	6.76 ± 0.62	6.99 ± 0.72	4.68 ± 0.65	6.04 ± 0.67

Veh, vehicle; ABL5, abaloparatide at 5 μg/kg/day; ABL25, abaloparatide at 25 μg/kg/day; MAR, mineral apposition rate; MS, mineralizing surface; BS, bone surface; BFR, bone formation rate; BV, bone volume.
^ $P < 0.05$ vs. Sham control.
* $P < 0.05$ vs. Veh control.
+ $P < 0.05$ vs. ABL5.

Trabecular BFR/BS was significantly greater in the ABL25 group compared with Veh controls, driven by higher MS/BS without a change in MAR (Fig. 3E–G). Trabecular MS/BS was also significantly higher in the ABL5 group vs Veh. The abaloparatide-related increases in trabecular BFR/BS and MS/BS are evident in the fluorescent photomicrographs of Fig. 2J–L, which show greater calcein labeling in the ABL5 and ABL25 groups compared with Veh. N.Ob/B.Pm (Fig. 3H) and Ob.S/BS (Table 1) were higher in the ABL25 group vs all other groups, whereas N.Oc/B.Pm was lower in the ABL5 group vs Veh and sham controls (Fig. 3I). Oc.S/BS, OS/BS and O.Th were similar in the abaloparatide

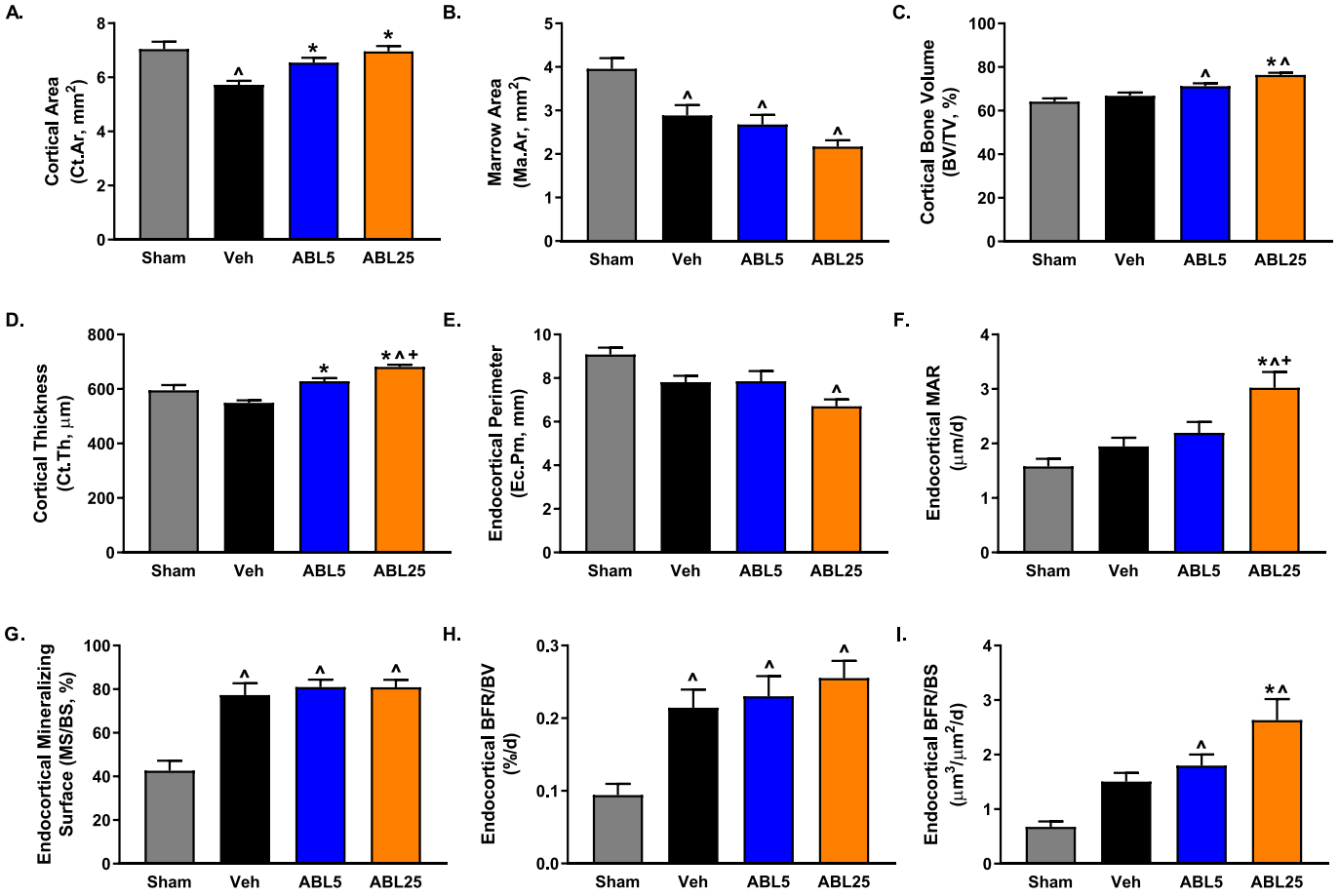

Fig. 1. Cortical bone histomorphometry for the tibial mid-diaphysis. See Table 1 for additional endpoints. Data represent means ± SEM, $N = 8$/group. ^$P < 0.05$ vs. Sham control; *$P < 0.05$ vs. Veh control; +$P < 0.05$ vs. ABL5. Abbreviations: TV, tissue volume; MAR, mineral apposition rate; BS, bone surface; BFR, bone formation rate; BV, bone volume.

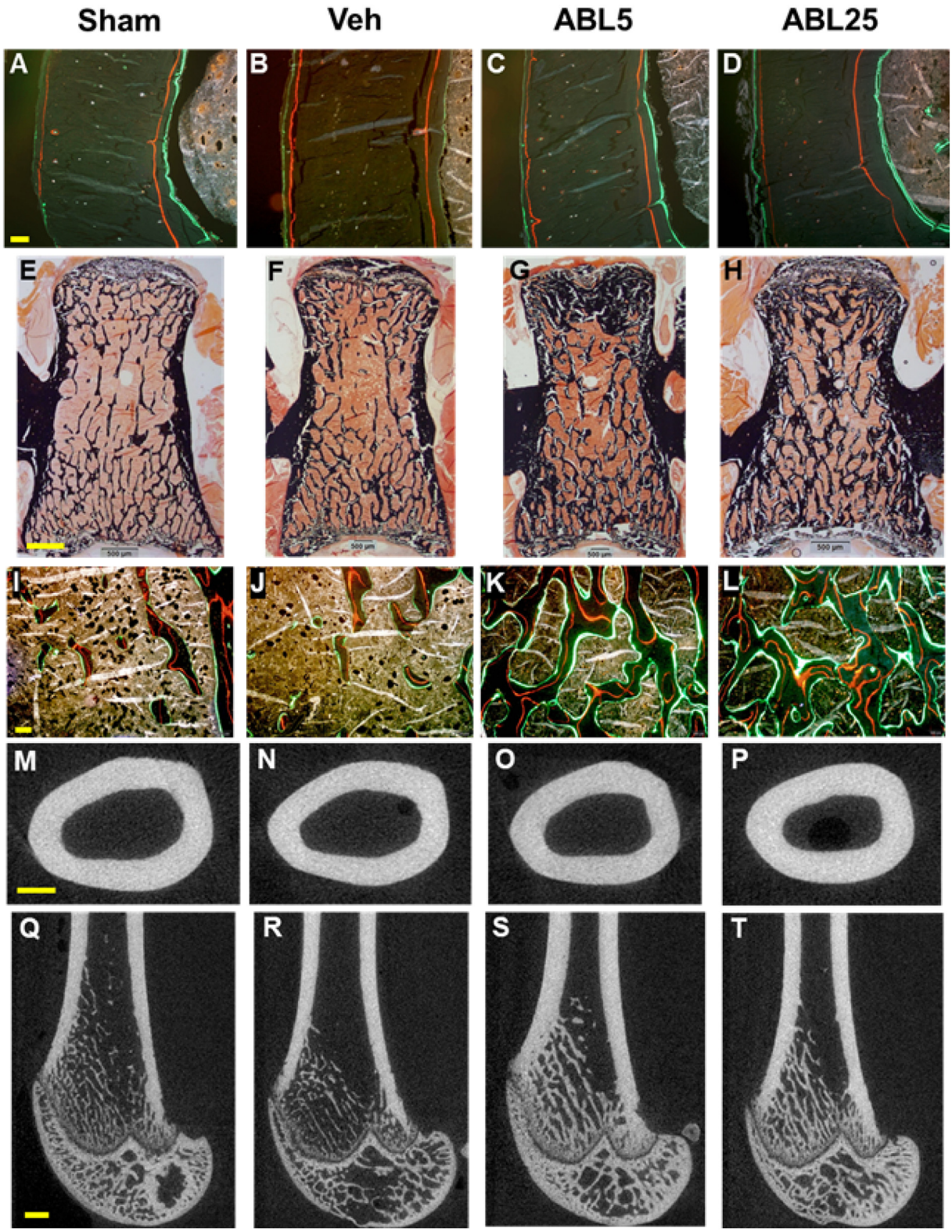

Fig. 2. Representative histology and micro-CT images from the Sham, Veh, ABL5, and ABL25 groups. **A-D**: Cross-sectional histology images of the tibial mid-diaphysis under fluorescence microscopy, with endocortical surface to the right. Regions of new bone formation are indicated by red (alizarin) labels and green (calcein) labels administered the week before treatment began and the last week of treatment, respectively. Yellow scale bar in D represents 100 μm. ***E*-H**: Von Kossa-stained histology sections of coronal sections of the L3 vertebral body, with black tissue representing mineralized bone matrix. Yellow scale bars in E-H represents 500 μm. **I-L**: Histology sections of L3 showing trabecular bone under high-magnification fluorescence microscopy, with alizarin red and calcein green labels indicating areas of new bone formation. Yellow scale bar in I represents 100 μm. **M-P**: Cross-sectional micro-CT images of the mid-femoral diaphysis. Yellow scale bar in L represents 1 mm. **Q-T**: Mid-sagittal micro-CT images of the distal femur. Yellow scale bar in Q represents 1 mm.

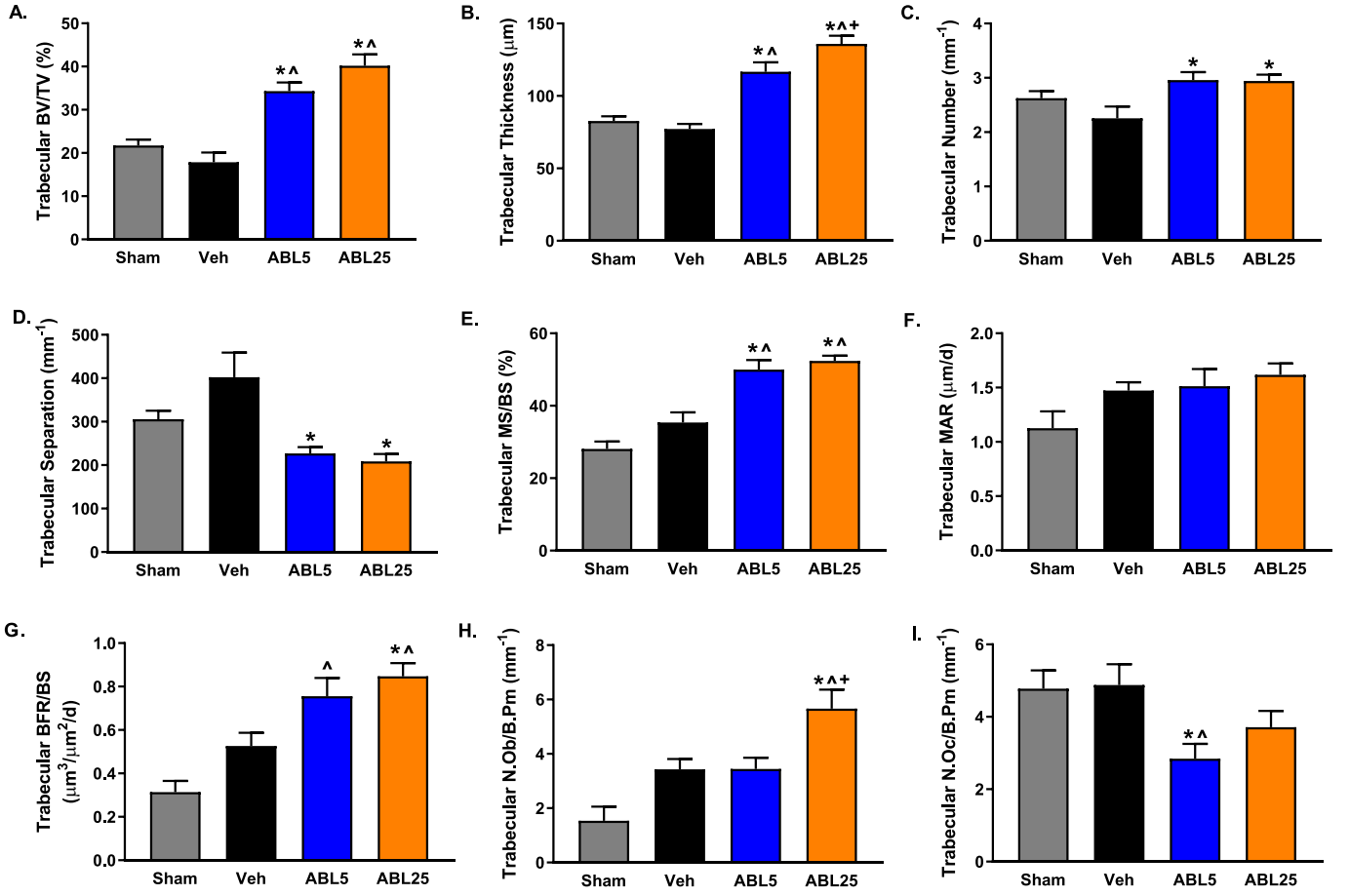

Fig. 3. Trabecular bone histomorphometry data for trabecular bone in the L3 vertebral body. See Table 1 for additional endpoints. Data represent means ± SEM, N = 8/group. $^{\wedge}P < 0.05$ vs. Sham control; $^{*}P < 0.05$ vs. Veh control; $^{+}P < 0.05$ vs. ABL5. Abbreviations: BV, bone volume; TV, tissue volume; MS, mineralizing surface; BS, bone surface; MAR, mineral apposition rate; BFR, bone formation rate; N, number; Ob, osteoblast; B.Pm, bone perimeter; Oc, osteoclast.

and Veh groups (Table 1).

3.3. Micro-CT

Micro-CT of the femoral mid-diaphysis showed that the Veh group had lower Tt.Ar, Ct.Ar, Ct.Th, and pMOI compared with Sham controls (Table 2). The ABL25 group showed significantly greater Ct.Ar/Tt.Ar and Ct.Th compared with Veh controls (Table 2), which is apparent in the micro-CT images shown in Fig. 2P vs N. There were no differences for either abaloparatide group vs Veh controls for femoral diaphyseal Tt.Ar, Ct.Ar, Ma.Ar, pMOI, Ct.TMD, or Ct.Po (Table 2). Total femur length in mm (mean ± SEM) at the end of the 8-week treatment period was 42.12 ± 0.32 in the Sham group, 40.39 ± 0.43 in the Veh group ($P < 0.05$ vs Sham), 40.93 ± 0.38 in the ABL5 group ($P = 0.06$ vs Sham), and 40.14 ± 0.29 in the ABL25 group ($P < 0.05$ vs. Sham); no significant differences were noted among the three ORX groups.

Micro-CT analyses also indicated significant ORX effects on trabecular bone in the distal femur, with lower Tb.vBMD, Tb.BV/TV, and Tb.N in the Veh group vs Sham controls (Fig. 4A, B, and D). The Veh group also had higher values for Tb.Sp compared with Sham controls (Fig. 4E). Both abaloparatide groups had higher Tb.vBMD, Tb.BV/TV, and Tb.Th, and lower SMI, compared with Veh controls (Fig. 4A–C and F). The ABL25 group also showed higher Tb.N and lower Tb.Sp vs. Veh controls (Fig. 4D–E). These structural improvements are apparent in representative micro-CT images shown in Fig. 2R-T.

Micro-CT of the L4 vertebral body showed that the Veh group had lower Tb.vBMD, Tb.BV/TV, Tb.N, and trabecular Conn.D, and higher Tb.Sp compared with Sham controls (Table 2). Both abaloparatide groups exhibited significantly greater L4 Tb.vBMD, Tb.BV/TV, Tb.Th, Tb.N, total bone area, total bone area per total area, and total vBMD, and significantly lower Tb.Sp and SMI compared with Veh controls (Table 2).

3.4. Bone biomechanics

Shear testing of the femoral neck indicated no significant differences between the Veh group and Sham controls for ultimate load, stiffness, or work to fracture (Fig. 5A–C). Both abaloparatide groups showed significantly greater femoral neck ultimate load vs Veh controls, and the ABL25 group's mean value also exceeded that of the Sham group (Fig. 5A). Three-point bending tests of the femoral diaphysis indicated significantly lower ultimate load and work to fracture in the Veh group vs Sham controls, and no differences between the abaloparatide and Veh groups (Fig. 5D–F). Estimated material properties of the femoral diaphysis showed no significant differences in apparent ultimate stress, apparent elastic modulus, and apparent toughness among the four groups (Fig. 5G–I).

Compressive testing of the L4 vertebral body indicated significantly greater ultimate load and work to ultimate load in both abaloparatide groups compared with Veh (Fig. 5J and L).

Potential strength determinants for the femoral diaphysis and L4 were evaluated in the ORX groups by linear regression analyses using structural parameters obtained by micro-CT. Femur diaphysis cortical area was a strong predictor of femoral diaphysis ultimate load across all groups ($r = 0.81$, $P < 0.0001$) and within the ABL5 ($r = 0.83$, $P = 0.003$) and ABL25 groups ($r = 0.74$, $P = 0.014$; Fig. 6A). Total

Table 2
Micro-CT data for the femoral diaphysis and L4 vertebral body. Data represent means ± SEM, $N = 10$/group.

	Sham	Veh	ABL5	ABL25
Femoral mid-diaphysis				
Total cross-sectional area (Tt.Ar, mm^2)	14.06 ± 0.61	11.86 ± 0.48^	11.95 ± 0.34^	11.50 ± 0.33^
Cortical area (Ct.Ar, mm^2)	8.76 ± 0.25	7.53 ± 0.19^	7.71 ± 0.13^	7.85 ± 0.13^
Marrow area (Ma.Ar, mm^2)	5.30 ± 0.40	4.33 ± 0.32	4.42 ± 0.25	3.65 ± 0.23^
Cortical area per total area (Ct.Ar/Tt.Ar, %)	62.7 ± 1.36	63.89 ± 1.23	64.71 ± 1.09	68.53 ± 1.17*^
Cortical thickness (Ct.Th, mm)	0.778 ± 0.014	0.731 ± 0.008^	0.751 ± 0.011	0.793 ± 0.012*
Polar moment of inertia (pMOI, mm^4)	28.47 ± 2.26	20.72 ± 1.47^	20.92 ± 1.00^	20.11 ± 1.03^
Tissue Mineral Density (TMD, mg/cm^3)	1149 ± 3.8	1162 ± 4.23	1156 ± 4.3	1160 ± 3.9
Cortical Porosity (Ct.Po, %)	0.496 ± 0.036	0.434 ± 0.021	0.404 ± 0.014^	0.405 ± 0.014^
L4 vertebral body				
Trabecular vBMD (Tb.vBMD, mg/cm^3)	422.6 ± 13.5	373.0 ± 13.9^	488.0 ± 13.29*^	526.2 ± 10.8*^
Trabecular BV/TV (Tb.BV/TV, %)	36.07 ± 1.83	29.58 ± 1.69^	45.01 ± 1.68*^	50.34 ± 1.58*^
Trabecular thickness (Tb.Th, mm)	0.090 ± 0.002	0.091 ± 0.002	0.117 ± 0.003*^	0.131 ± 0.002*^+
Trabecular number (Tb.N, mm^{-1})	4.24 ± 0.20	3.31 ± 0.16^	4.01 ± 0.14*	4.12 ± 0.13*
Connectivity Density (Conn.D)	97.47 ± 5.74	59.68 ± 3.21^	50.06 ± 2.97^	45.93 ± 3.22^
Trabecular separation (Tb.Sp, mm)	0.233 ± 0.015	0.306 ± 0.018^	0.239 ± 0.010*	0.228 ± 0.011*
Trabecular structure model index (SMI)	−0.32 ± 0.18	0.28 ± 0.12	−1.22 ± 0.20*^	−1.76 ± 0.23*^
Total bone area (Tt.B.Ar, mm^2)	7.85 ± 0.29	6.76 ± 0.31	8.44 ± 0.28*	9.04 ± 0.29*^
Total bone area per total area (Tt.B.Ar/Tt.Ar, %)	55.1 ± 1.8	50.7 ± 1.5	64.8 ± 1.5*^	69.8 ± 1.7*^
Total vBMD (Tt.vBMD, mg/cm^3)	562.0 ± 13.2	534.7 ± 11.7	636.9 ± 13.5*^	671.6 ± 14.0*^

Veh, vehicle; ABL5, abaloparatide at 5 μg/kg/day; ABL25, abaloparatide at 25 μg/kg/day; vBMD, volumetric bone mineral density; BV, bone volume; TV, total volume.
^ $P < 0.05$ vs. Sham control.
* $P < 0.05$ vs. Veh control.
+ $P < 0.05$ vs. ABL5.

bone area of L4 was a strong predictor of L4 ultimate load, with an r value of 0.76 across all groups ($P < 0.0001$) and an r value of 0.80 in the ABL25 group ($P = 0.006$; Fig. 6B). L4 Tb.BV/TV also predicted L4 ultimate load, with an overall r value of 0.75 ($P < 0.0001$) (regression not shown).

4. Discussion

Androgen deficiency in men can lead to increased bone resorption and reduced bone formation, leading to deterioration of cortical and trabecular bone and an increase in fracture risk [19,31–34]. The current male rat study assessed the ability of the osteoanabolic agent abaloparatide to reverse the adverse skeletal effects of abrupt, sustained androgen deprivation caused by surgical castration.

Cortical bone histomorphometry at the tibial diaphysis showed that one or both abaloparatide groups had significantly greater cortical bone area, cortical BV/TV, cortical thickness, endocortical MAR, endocortical BFR/BS, periosteal MS/BS, and intracortical BFR compared with Veh controls. Previous longitudinal pQCT data from this study showed that increased tibial diaphyseal cortical thickness with abaloparatide was primarily related to its effect of preventing endocortical expansion [28], and the current histomorphometry analyses identify increased endocortical bone formation as the likely mechanism for cortical gains in these ORX rats.

Similar to findings in abaloparatide-treated OVX monkeys [5], abaloparatide treatment did not increase cortical porosity in these ORX

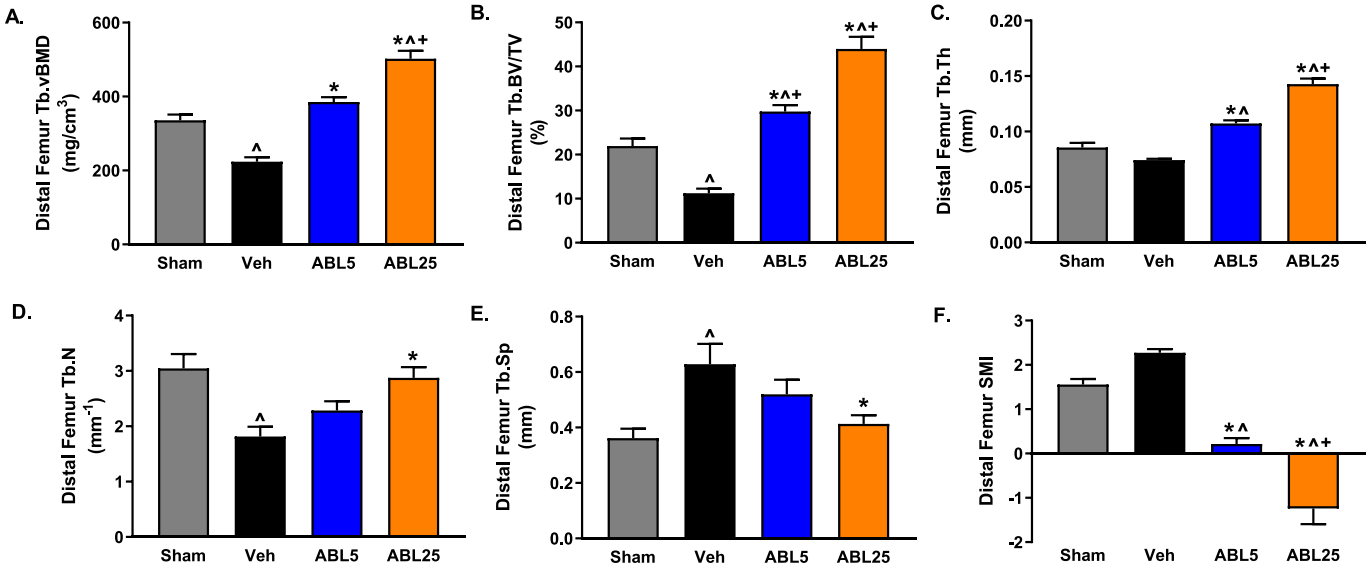

Fig. 4. Distal femur trabecular micro-CT. Data represent means ± SEM, $N = 10$/group. ^$P < 0.05$ vs. Sham control; *$P < 0.05$ vs. Veh control; +$P < 0.05$ vs. ABL5. Abbreviations: Tb, trabecular; BV, bone volume; TV, total volume; vBMD, volumetric bone mineral density; SMI, structural model index; N, number; Th, thickness; Sp, separation.

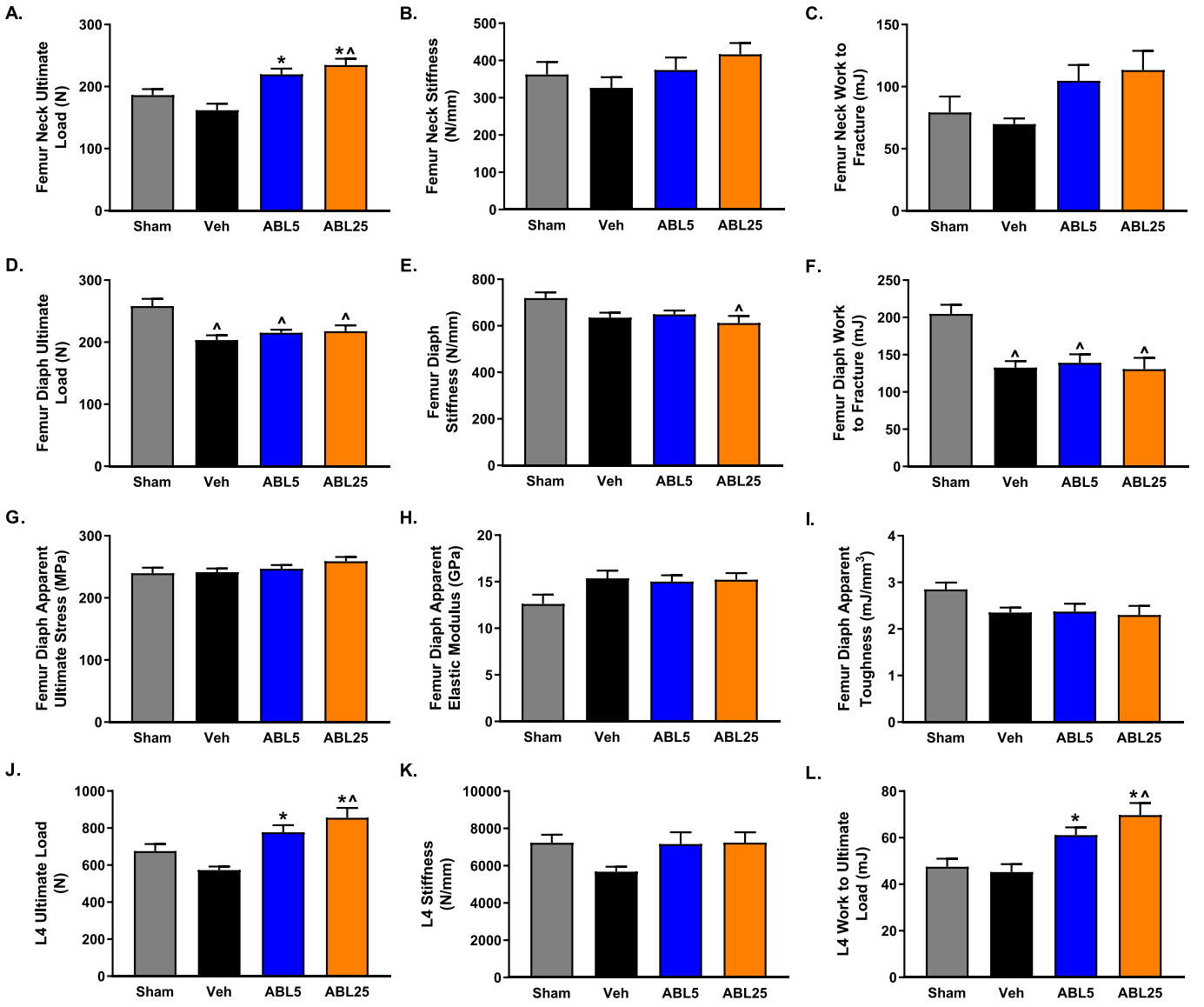

Fig. 5. Bone biomechanics for the femoral neck tested in shear (A-C), the femoral diaphysis tested in 3-point bending, (D-I), and the 4th lumbar vertebral body (L4) tested in compression (J-L). Data represent means ± SEM, N = 10/group. ^$P < 0.05$ vs. Sham control; *$P < 0.05$ vs. Veh control.

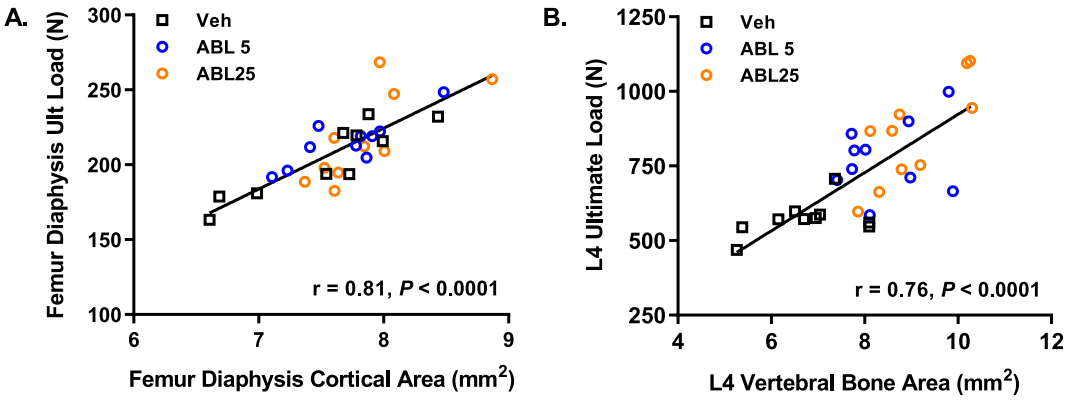

Fig. 6. Bone mass-strength relationships for the femur diaphysis and 4th lumbar vertebral body from the 3 OVX groups (Veh, vehicle; ABL5, abaloparatide 5 μg/kg/d; ABL25, abaloparatide 25 μg/kg/d). A) Femur diaphysis ultimate load in 3-point bending was linearly related to micro-CT-derived femur diaphysis cortical area. B) L4 compressive ultimate load was linearly related to micro-CT-derived L4 bone area. R values listed in the figures represent regression lines for all 3 groups combined, based on statistical findings of no significant differences among the groups for slopes and intercepts.

rats. Increased cortical porosity in teriparatide-treated OVX monkeys has been attributed to increased intracortical bone turnover [35], and the lack of increased porosity in these abaloparatide-treated ORX rats may reflect an underlying resistance of rats to intracortical remodeling. Interestingly though, intracortical bone formation rate was significantly increased in the ABL25 group compared with Veh controls, and this effect may have minimized cortical porosity by accelerating osteon refilling, as previously described [36]. Consistent with that hypothesis, increased cortical porosity in teriparatide-treated OVX monkeys was associated with a lack of increased intracortical bone formation [35]. It should be noted that abaloparatide and teriparatide both increased cortical porosity in iliac crest bone biopsies obtained from postmenopausal women with osteoporosis [37], though the clinical relevance of those findings, obtained from a non-weight-bearing skeletal site, remains unclear. The generalizability of increased cortical porosity observed at the iliac crest to other skeletal sites is also uncertain, based on evidence that non-weight-bearing bones may be more susceptible to increased porosity compared with weight-bearing bones [36,38].

The femoral diaphysis of the ABL25 group had greater cortical thickness vs Veh controls by micro-CT, likely due to non-significantly lower marrow area because total diaphyseal cross-sectional area was not increased. Increased cortical thickness would be a desirable therapeutic response in men with osteoporosis, for whom cortical thinning represents an important adverse structural change [39]. Despite greater cortical thickness, femoral diaphysis bending strength was not significantly higher in the ABL25 group compared with Veh controls. Data previously reported for this study showed progressively greater mid-femur areal BMD gains in the ABL25 group versus Veh controls throughout the 8-week treatment period [28], and the ABL25 group from a previous OVX rat study showed progressively greater mid-femur BMD gains throughout a 12-month treatment period [6]. Those data suggest the possibility that a longer duration of abaloparatide treatment may lead to additional BMD gains that could eventually increase femoral diaphysis strength in ORX rats. But ultimately the lack of greater femoral diaphyseal cross-sectional area after 8 weeks of abaloparatide in these ORX rats probably explains the lack of increased femur bending strength. Previous analyses of the femur periosteum of growing ORX rats indicated that fluorochrome labeling was minimal with or without 12 weeks of teriparatide administration [40]. In contrast to the current results, abaloparatide promoted progressive periosteal expansion of the femoral diaphysis in OVX rats, a model wherein gonadectomy itself did not impair periosteal expansion [6]. These findings suggest that ORX-related suppression of periosteal apposition may have partially blunted periosteal responsiveness to abaloparatide, though greater periosteal MS/BS indicates that the ORX rat periosteum retained some responsiveness to abaloparatide. Femur length data from the current study indicate that ORX also inhibited longitudinal bone growth, an effect that was not reversed by abaloparatide. Taken together, these results indicate that the long bone phenotype of growing ORX rats diverges from that of elderly men, in whom long bones tend to undergo radial expansion with age, though not enough to prevent the cortical thinning that results from progressive endocortical expansion [10,39]. Periosteal bone formation can remain suppressed in ORX rats as old as 8–12 months of age [41], and it would be interesting to evaluate whether abaloparatide or other PTHR agonists are capable of stimulating periosteal apposition in ORX rats beyond those ages.

Trabecular bone histomorphometry indicated that abaloparatide increased dynamic parameters of bone formation in the vertebra, where it also increased osteoblast numbers without increasing osteoclast numbers. Those findings, and the accompanying improvements in trabecular bone volume and micro-architecture, are consistent with proximal tibial trabecular histomorphometry results from this study [28], and indicate that abaloparatide augments trabecular bone in both the axial and appendicular ORX rat skeleton. Previous tibial pQCT data showed that trabecular bone in these ORX rats was deficient versus sham controls prior to initiating abaloparatide treatment [28], indicating that abaloparatide can reverse established trabecular osteopenia caused by androgen deficiency. The results of regression analyses suggest that abaloparatide-induced gains in trabecular bone volume contributed to improved vertebral strength, though possible contributions from an augmented vertebral cortex cannot be ruled out, as total L4 bone area was an equally strong predictor of L4 strength.

The ABL5 and ABL25 groups showed higher femoral neck strength, with ultimate load values significantly exceeding those of Veh and Sham controls. It was previously reported that the ABL5 and ABL25 groups exhibited significantly greater gains in proximal femur aBMD compared with Veh and Sham controls [28], suggesting a structural basis for increased femoral neck strength. That possibility is also supported by prior evidence that improved femoral neck strength in abaloparatide-treated OVX rats was associated with increases in proximal femur aBMC [6]. Abaloparatide also increases femoral neck BMD in OVX monkeys [5] and in women with postmenopausal osteoporosis [3]. Increases in hip BMD and hip strength are important goals for osteoporosis therapy in elderly men, many of whom experience sharp decreases in hip and femoral neck BMD in their 8th decade [10].

This study has several limitations. These rats were still undergoing longitudinal and periosteal bone growth, both of which were suppressed by ORX, which represents a divergence from the skeletal phenotype of elderly men, who generally show age-related periosteal expansion of long bones [10,39]. ORX rats may be a less-than-optimal animal model for forms of male osteoporosis that develop through gradual age-associated reductions in androgen levels. ORX rats experience rapid and profound reductions in androgen levels [26], similar to the effects of surgical or medical androgen deprivation therapy in patients with prostate cancer, a disease these rats did not have. Serum testosterone levels were not assessed in the current study, though a state of androgen deprivation was supported by ORX-related deficits in weight gain and by the typical ORX-related bone changes observed vs Sham controls. The duration of treatment was relatively brief and may not predict the skeletal effects of longer-term abaloparatide therapy in androgen-deficient states.

In summary, abaloparatide treatment of ORX rats was associated with increased bone formation parameters in endocortical, intracortical, periosteal, and trabecular envelopes, leading to improved bone mass, cortical geometry, and trabecular micro-architecture. Increased vertebral and femoral neck strength in these abaloparatide-treated ORX rats provides a further preclinical rationale for exploring abaloparatide as an investigational therapy for male osteoporosis.

Conflicts of interest

Authors TB, MO, BM, GH, and BL are current or former employees of Radius Health. RB has been a consultant and a member of advisory boards for Radius Health.

Acknowledgements

Funding for this work was provided by Radius Health Inc. Medical writing support was provided by Paul Kostenuik, PhD, of Phylon Pharma Services.

References

[1] S. Gonnelli, C. Caffarelli, Abaloparatide, Clin Cases Miner Bone Metab 13 (2016) 106–109.
[2] G. Hattersley, T. Dean, B.A. Corbin, H. Bahar, T.J. Gardella, Binding selectivity of abaloparatide for PTH-type-1-receptor conformations and effects on downstream signaling, Endocrinology 157 (2016) 141–149.
[3] P.D. Miller, G. Hattersley, B.J. Riis, G.C. Williams, E. Lau, L.A. Russo, P. Alexandersen, C.A. Zerbini, M.Y. Hu, A.G. Harris, L.A. Fitzpatrick, F. Cosman, C. Christiansen, A.S. Investigators, Effect of abaloparatide vs placebo on new vertebral fractures in postmenopausal women with osteoporosis: a randomized clinical trial, JAMA 316 (2016) 722–733.
[4] F. Cosman, P.D. Miller, G.C. Williams, G. Hattersley, M.Y. Hu, I. Valter,

L.A. Fitzpatrick, B.J. Riis, C. Christiansen, J.P. Bilezikian, D. Black, Eighteen months of treatment with subcutaneous abaloparatide followed by 6 months of treatment with alendronate in postmenopausal women with osteoporosis: results of the ACTIVExtend trial, Mayo Clin. Proc. 92 (2017) 200–210.
[5] N. Doyle, A. Varela, S. Haile, R. Guldberg, P.J. Kostenuik, M.S. Ominsky, S.Y. Smith, G. Hattersley, Abaloparatide, a novel PTH receptor agonist, increased bone mass and strength in ovariectomized cynomolgus monkeys by increasing bone formation without increasing bone resorption, Osteoporos. Int. 29 (2018) 685–697.
[6] A. Varela, L. Chouinard, E. Lesage, R. Guldberg, S.Y. Smith, P.J. Kostenuik, G. Hattersley, One year of abaloparatide, a selective peptide activator of the PTH1 receptor, increased bone mass and strength in ovariectomized rats, Bone 95 (2017) 143–150.
[7] A. Varela, L. Chouinard, E. Lesage, S.Y. Smith, G. Hattersley, One year of abaloparatide, a selective activator of the PTH1 receptor, increased bone formation and bone mass in osteopenic ovariectomized rats without increasing bone resorption, J. Bone Miner. Res. 32 (2017) 24–33.
[8] M. Laurent, E. Gielen, F. Claessens, S. Boonen, D. Vanderschueren, Osteoporosis in older men: recent advances in pathophysiology and treatment, Best Practice Res Clinical Endocrinol Metabol 27 (2013) 527–539.
[9] R.A. Adler, Osteoporosis in men: a review, Bone Res 2 (2014) 14001.
[10] P. Szulc, P.D. Delmas, Bone loss in elderly men: increased endosteal bone loss and stable periosteal apposition. The prospective MINOS study, Osteoporos. Int. 18 (2007) 495–503.
[11] A. Falahati-Nini, B.L. Riggs, E.J. Atkinson, W.M. O'Fallon, R. Eastell, S. Khosla, Relative contributions of testosterone and estrogen in regulating bone resorption and formation in normal elderly men, J. Clin. Invest. 106 (2000) 1553–1560.
[12] D. McLeod, N. Zinner, K. Tomera, D. Gleason, N. Fotheringham, M. Campion, M.B. Garnick, G. Abarelix Study, A phase 3, multicenter, open-label, randomized study of abarelix versus leuprolide acetate in men with prostate cancer, Urology 58 (2001) 756–761.
[13] V.B. Shahinian, Y.F. Kuo, J.L. Freeman, J.S. Goodwin, Risk of fracture after androgen deprivation for prostate cancer, N. Engl. J. Med. 352 (2005) 154–164.
[14] S.M. Harman, E.J. Metter, J.D. Tobin, J. Pearson, M.R. Blackman, Longitudinal effects of aging on serum total and free testosterone levels in healthy men, J. Clin. Endocrinol. Metab. 86 (2001) 724–731.
[15] G. Sartorius, S. Spasevska, A. Idan, L. Turner, E. Forbes, A. Zamojska, C.A. Allan, L.P. Ly, A.J. Conway, R.I. McLachlan, D.J. Handelsman, Serum testosterone, dihydrotestosterone and estradiol concentrations in older men self-reporting very good health: the healthy man study, Clin. Endocrinol. 77 (2012) 755–763.
[16] G. Golds, D. Houdek, T. Arnason, Male hypogonadism and osteoporosis: the effects, clinical consequences, and treatment of testosterone deficiency in bone health, Int. J. Endocrinol. 2017 (2017) 4602129.
[17] T.G. Travison, A.B. Araujo, A.B. O'Donnell, V. Kupelian, J.B. McKinlay, A population-level decline in serum testosterone levels in American men, J. Clin. Endocrinol. Metab. 92 (2007) 196–202.
[18] P. Szulc, B. Claustrat, F. Marchand, P.D. Delmas, Increased risk of falls and increased bone resorption in elderly men with partial androgen deficiency: the MINOS study, J. Clin. Endocrinol. Metab. 88 (2003) 5240–5247.
[19] O. Johnell, J.A. Kanis, An estimate of the worldwide prevalence and disability associated with osteoporotic fractures, Osteoporos. Int. 17 (2006) 1726–1733.
[20] J.R. Center, T.V. Nguyen, D. Schneider, P.N. Sambrook, J.A. Eisman, Mortality after all major types of osteoporotic fracture in men and women: an observational study, Lancet 353 (1999) 878–882.
[21] P. Haentjens, J. Magaziner, C.S. Colon-Emeric, D. Vanderschueren, K. Milisen, B. Velkeniers, S. Boonen, Meta-analysis: excess mortality after hip fracture among older women and men, Ann. Intern. Med. 152 (2010) 380–390.
[22] A.C. Feldstein, G. Nichols, E. Orwoll, P.J. Elmer, D.H. Smith, M. Herson, M. Aickin, The near absence of osteoporosis treatment in older men with fractures, Osteoporos. Int. 16 (2005) 953–962.
[23] E.S. Orwoll, W.H. Scheele, S. Paul, S. Adami, U. Syversen, A. Diez-Perez, J.M. Kaufman, A.D. Clancy, G.A. Gaich, The effect of teriparatide [human parathyroid hormone (1-34)] therapy on bone density in men with osteoporosis, J. Bone Miner. Res. 18 (2003) 9–17.
[24] F.R. Ricarte, C. Le Henaff, V.G. Kolupaeva, T.J. Gardella, N.C. Partridge, Parathyroid hormone(1-34) and its analogs differentially modulate osteoblastic Rankl expression via PKA/SIK2/SIK3 and PP1/PP2A-CRTC3 signaling, J. Biol. Chem. 293 (2018) 20200–20213.
[25] A. Makino, H. Takagi, Y. Takahashi, N. Hase, H. Sugiyama, K. Yamana, T. Kobayashi, Abaloparatide exerts one anabolic effects with less stimulation of bone resorption-related factors: a comparison with teriparatide, Calcif. Tissue Int. 103 (2018) 289–297.
[26] X. Li, M.S. Ominsky, M. Stolina, K.S. Warmington, Z. Geng, Q.T. Niu, F.J. Asuncion, H.L. Tan, M. Grisanti, D. Dwyer, S. Adamu, H.Z. Ke, W.S. Simonet, P.J. Kostenuik, Increased RANK ligand in bone marrow of orchiectomized rats and prevention of their bone loss by the RANK ligand inhibitor osteoprotegerin, Bone 45 (2009) 669–676.
[27] V. Proell, H. Xu, C. Schuler, K. Weber, L.C. Hofbauer, R.G. Erben, Orchiectomy upregulates free soluble RANKL in bone marrow of aged rats, Bone 45 (2009) 677–681.
[28] H. Chandler, B. Lanske, A. Varela, M. Guillot, M. Boyer, J. Brown, A. Pierce, M. Ominsky, B. Mitlak, R. Baron, P. Kostenuik, G. Hattersley, Abaloparatide, a novel osteoanabolic PTHrP analog, increases cortical and trabecular bone mass and architecture in orchiectomized rats by increasing bone formation without increasing bone resorption, Bone 120 (2019) 148–155.
[29] D.W. Dempster, J.E. Compston, M.K. Drezner, F.H. Glorieux, J.A. Kanis, H. Malluche, P.J. Meunier, S.M. Ott, R.R. Recker, A.M. Parfitt, Standardized nomenclature, symbols, and units for bone histomorphometry: a 2012 update of the report of the ASBMR Histomorphometry nomenclature committee, J. Bone Miner. Res. 28 (2013) 2–17.
[30] M.L. Bouxsein, S.K. Boyd, B.A. Christiansen, R.E. Guldberg, K.J. Jepsen, R. Muller, Guidelines for assessment of bone microstructure in rodents using micro-computed tomography, J. Bone Miner. Res. 25 (2010) 1468–1486.
[31] R. Burge, B. Dawson-Hughes, D.H. Solomon, J.B. Wong, A. King, A. Tosteson, Incidence and economic burden of osteoporosis-related fractures in the United States, 2005-2025, J. Bone Miner. Res. 22 (2007) 465–475.
[32] M.R. Smith, F. Saad, S. Chowdhury, S. Oudard, B.A. Hadaschik, J.N. Graff, D. Olmos, P.N. Mainwaring, J.Y. Lee, H. Uemura, A. Lopez-Gitlitz, G.C. Trudel, B.M. Espina, Y. Shu, Y.C. Park, W.R. Rackoff, M.K. Yu, E.J. Small, S. Investigators, Apalutamide treatment and metastasis-free survival in prostate cancer, N. Engl. J. Med. 378 (2018) 1408–1418.
[33] Y. Pernow, B. Granberg, M. Saaf, L. Weidenhielm, Osteoblast dysfunction in male idiopathic osteoporosis, Calcif. Tissue Int. 78 (2006) 90–97.
[34] Y. Pernow, E.M. Hauge, K. Linder, E. Dahl, M. Saaf, Bone histomorphometry in male idiopathic osteoporosis, Calcif. Tissue Int. 84 (2009) 430–438.
[35] D.B. Burr, T. Hirano, C.H. Turner, C. Hotchkiss, R. Brommage, J.M. Hock, Intermittently administered human parathyroid hormone(1-34) treatment increases intracortical bone turnover and porosity without reducing bone strength in the humerus of ovariectomized cynomolgus monkeys, J. Bone Miner. Res. 16 (2001) 157–165.
[36] M.S. Ominsky, S.K. Boyd, A. Varela, J. Jolette, M. Felx, N. Doyle, N. Mellal, S.Y. Smith, K. Locher, S. Buntich, I. Pyrah, R.W. Boyce, Romosozumab improves bone mass and strength while maintaining bone quality in ovariectomized cynomolgus monkeys, J. Bone Miner. Res. 32 (2017) 788–801.
[37] C.A. Moreira, L.A. Fitzpatrick, Y. Wang, R.R. Recker, Effects of abaloparatide-SC (BA058) on bone histology and histomorphometry: the ACTIVE phase 3 trial, Bone 97 (2017) 314–319.
[38] P.J. Kostenuik, S.Y. Smith, J. Jolette, J. Schroeder, I. Pyrah, M.S. Ominsky, Decreased bone remodeling and porosity are associated with improved bone strength in ovariectomized cynomolgus monkeys treated with denosumab, a fully human RANKL antibody, Bone 49 (2011) 151–161.
[39] L.M. Marshall, T.F. Lang, L.C. Lambert, J.M. Zmuda, K.E. Ensrud, E.S. Orwoll, O.F.i.M.R. Group, Dimensions and volumetric BMD of the proximal femur and their relation to age among older U.S. men, J. Bone Miner. Res. 21 (2006) 1197–1206.
[40] Y. Gabet, D. Kohavi, R. Muller, M. Chorev, I. Bab, Intermittently administered parathyroid hormone 1-34 reverses bone loss and structural impairment in orchiectomized adult rats, Osteoporos. Int. 16 (2005) 1436–1443.
[41] H.Z. Ke, D.T. Crawford, H. Qi, K.L. Chidsey-Frink, H.A. Simmons, M. Li, W.S. Jee, D.D. Thompson, Long-term effects of aging and orchidectomy on bone and body composition in rapidly growing male rats, J. Musculoskelet. Neuronal Interact. 1 (2001) 215–224.